

# Reassessment of the Limiting Efficiency for Crystalline Silicon Solar Cells

Armin Richter, Martin Hermle, and Stefan W. Glunz, *Member, IEEE*

**Abstract**—Recently, several parameters relevant for modeling crystalline silicon solar cells were improved or revised, e.g., the international standard solar spectrum or properties of silicon such as the intrinsic recombination rate and the intrinsic carrier concentration. In this study, we analyzed the influence of these improved state-of-the-art parameters on the limiting efficiency for crystalline silicon solar cells under 1-sun illumination at 25 °C, by following the narrow-base approximation to model ideal solar cells. We also considered bandgap narrowing, which was not addressed so far with respect to efficiency limitation. The new calculations that are presented in this study result in a maximum theoretical efficiency of 29.43% for a 110-μm-thick solar cell made of undoped silicon. A systematic calculation of the  $I$ - $V$  parameters as a function of the doping concentration and the cell thickness together with an analysis of the loss current at maximum power point provides further insight into the intrinsic limitations of silicon solar cells.

**Index Terms**—Efficiency limit, silicon, solar cells.

## I. INTRODUCTION

THE maximum power conversion efficiency of silicon solar cells is limited by the intrinsic properties of silicon, such as the bandgap energy or the charge carrier recombination properties. This intrinsic limitation is of basic interest for PV research, particularly as continuous improvements in technology lead to solar cell operation conditions approaching this fundamental limit, e.g., the open-circuit voltage of heterojunction silicon solar cells [1].

Based on the detailed balancing of incident and generated power density, Shockley and Queisser determined an upper efficiency limit for ideal single-junction solar cells taking only radiative recombination into account [2]. In crystalline silicon, however, there are also considerable nonradiative intrinsic loss processes, in particular Auger recombination or parasitic free-carrier absorption (FCA). By calculating the limiting efficiency including nonradiative losses, both Green [3] and Tiedje *et al.* [4] showed that actually Auger recombination is the dominant intrinsic loss mechanism for c-Si solar cells at 1-sun illumination. Both even underestimated the Auger recombination as they used

the traditional free-particle model, which accounts not for the increased recombination probability that is caused by Coulomb interactions of electron and holes [5]. Kerr *et al.* addressed the effect of this Coulomb-enhanced Auger recombination on the limiting efficiency [6] by applying their general parameterization of the intrinsic recombination rate [7], which results in a maximum efficiency of 29.05% for solar cells made of undoped silicon.

Subsequently, the quantitative description of the radiative and the Auger recombination was improved further. Trupke *et al.* measured thoroughly the radiative recombination coefficient  $B$  [8], which appeared to be 50% smaller than the value used by Kerr *et al.* [6], [7], and Altermatt *et al.* extended the radiative recombination model by Coulomb interactions [9] similar to the Coulomb-enhanced Auger recombination. The Auger recombination, according to the most commonly used parameterization of Kerr and Cuevas [7], was found to be significantly overestimated for lowly doped silicon ( $<10^{16}$  cm $^{-3}$ ) [10], which is relevant for the optimum c-Si solar cell. Taking the Coulomb-enhanced radiative recombination into account, an improved parameterization for the intrinsic bulk lifetime was introduced in [10].

Besides these intrinsic recombination properties, other parameters relevant for the efficiency limit of c-Si solar cells were recently improved: 1) A new internationally accepted reference solar spectrum was introduced [11], which led to a significant increase of revised experimental solar cell peak efficiencies [12]; 2) Green presented self-consistent optical parameters of intrinsic silicon that are based on improved experimental data [13]; and 3) Rüdiger *et al.* determined new parameters for FCA explicitly for a wavelength range below 2 μm [14], the relevant range for c-Si solar cells.

Furthermore, Mattheis *et al.* showed that the charge carrier mobility causes no inherent limitation to the maximum efficiency as is the case, e.g., for solar cells with amorphous silicon base [15]. The influence of bandgap narrowing (BGN) on the limiting efficiency, however, has not been addressed so far. BGN affects the effective intrinsic carrier concentration  $n_{i,\text{eff}}$ , which increases considerably with increasing charge carrier concentration, in particular with increasing injection level [16], [17] (cf., Fig. 1). The  $I$ - $V$  characteristic of silicon solar cells is a function of  $n_{i,\text{eff}}^2$  and, thus, depends sensitively on  $n_{i,\text{eff}}$ . Therefore, BGN becomes not only important for high base doping concentrations, but also for low base doping concentrations under high injection [18], as is the case for the optimum silicon solar cell.

In this paper, we calculated the limiting efficiency for single junction silicon solar cells under 1-sun illumination (AM1.5G) at 25 °C based on state-of-the-art modeling parameters. In

Manuscript received April 9, 2013; revised May 17, 2013; accepted May 30, 2013. Date of publication July 10, 2013; date of current version September 18, 2013. This work was supported by the German Federal Ministry for the Environment, Nature Conservation, and Nuclear Safety under Contract 0325292 “ForTeS.”

The authors are with the Fraunhofer Institute for Solar Energy Systems, Freiburg 79110, Germany (e-mail: armin.richter@ise.fraunhofer.de; martin.hermle@ise.fraunhofer.de; stefan.glunz@ise.fraunhofer.de).

Color versions of one or more of the figures in this paper are available online at <http://ieeexplore.ieee.org>.

Digital Object Identifier 10.1109/JPHOTOV.2013.2270351

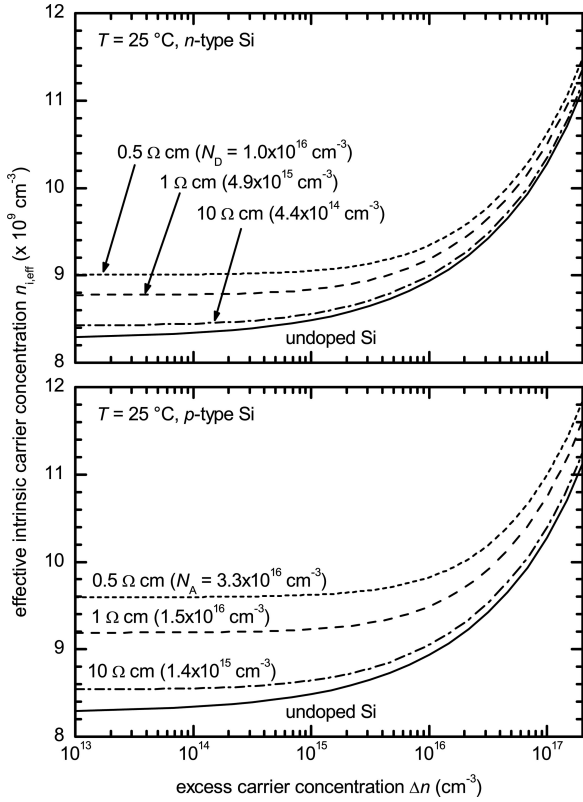


Fig. 1. Effective intrinsic carrier concentration  $n_{i,\text{eff}}$  for n-type Si (upper graph), and p-type Si (lower graph) at 25 °C as a function of  $\Delta n$  for different base doping concentrations.  $n_{i,\text{eff}}$  is calculated according to [16], [17], and [19] as described in Section II-D.

doing so, we address the effect on the efficiency limit for each parameter separately, which differs from the frequently cited calculations of Kerr *et al.* [6]. These are 1) the new solar spectrum; 2) the updated optical properties of silicon; 3) the new parameters for FCA; 4) the improved description of radiative and Auger recombination; and 5) the effect of BGN. Finally, we investigate in detail, the limiting efficiency as a function of the base doping concentration and the wafer thickness.

## II. MODELING OF THE I–V CHARACTERISTIC

### A. General Approach

To determine the maximum efficiency of silicon solar cells limited by the intrinsic properties of silicon, we follow the approach of previous publications in modeling ideal cells without surface and defect recombination, as well as perfect front-side antireflection coatings and perfect reflecting rear mirrors [4], [6], [20]. In doing so, we do not consider any efficiency enhancement associated with impurity bands, improved internal confinement due to quantum structures, or spectrum-shifting (up or down conversion). The current–voltage characteristic of such an ideal cell can be expressed as

$$J = J_L - qWR_{\text{intr}} \quad (1)$$

where  $J_L$  is the current density that is generated by the incident light,  $W$  the cell thickness,  $R_{\text{intr}}$  the intrinsic recombination

rate (radiative and Auger recombination), and  $q$  the elementary charge. The intrinsic bulk lifetime of silicon  $\tau_{\text{intr}}$  and, consequently, also  $R_{\text{intr}} = \Delta n/\tau_{\text{intr}}$  is an explicit function of the excess carrier concentration  $\Delta n$ . Under the assumption of a “narrow base,” the change of the quasi-Fermi levels within the base is very small, and the quasi-Fermi level separation can be considered to be constant [3]. When assuming additionally ideal contacts, the quasi-Fermi level separation equals the cells output voltage  $V$ , and thus,  $\Delta n$  is related to  $V$  by [3], [4]

$$np = (n_0 + \Delta n)(p_0 + \Delta n) = n_{i,\text{eff}}^2 \exp\left(\frac{qV}{k_B T}\right) \quad (2)$$

with the electron and hole concentrations  $n$  and  $p$ , the respective equilibrium concentrations  $n_0$  and  $p_0$ , the Boltzmann constant  $k_B$ , and the temperature  $T$ . This relation is used to determine  $\Delta n(V, n_0, p_0)$  for  $R_{\text{intr}}(n_0, p_0, \Delta n)$  in (1). Actually, (1) is also based on the narrow base assumption as it implies a constant recombination rate throughout the cell, which is fulfilled if the quasi-Fermi levels are constant. It should be mentioned that by modeling the I–V characteristic with (1), we assume in addition to ideal contacts also negligible series resistance losses arising from the charge carrier transport within the silicon bulk. Obviously, this is a good assumption for cells made of highly doped silicon. However, it is also a good assumption for cells made of lowly doped silicon, as these are in sufficient high injection at maximum power point (mpp) (cf., Section III-B).

### B. Photogeneration

The absorbed current density  $J_L$  was calculated assuming that every photon absorption event generates a single electron–hole pair. The creation of multiple electron–hole pairs by high-energy photons [21] was neglected, as it is a quite small effect, contributing less than 0.1 mA/cm<sup>2</sup> [20], [22]. Further, a Lambertian randomizing light-trapping scheme together with an isotropic response of the cell was assumed, which results in an increased mean path length for a light ray inside the cell of  $4n_r^2 W$ , where  $n_r$  is the refractive index of silicon [4]. The weakly absorbed subbandgap photons have also a certain probability of being absorbed by free carriers. Taking this parasitic FCA into account,  $J_L$  can be determined from

$$J_L = q \int_0^\infty A_{\text{bb}}(E) \Phi(E) dE \quad (3)$$

with the spectrally resolved relative absorbance in the cell [4]

$$A_{\text{bb}}(E) = \frac{\alpha_{\text{bb}}(E)}{\alpha_{\text{bb}}(E) + \alpha_{\text{FCA}}(E) + \frac{1}{4n_r^2 W}} \quad (4)$$

the solar spectrum  $\Phi$  normalized to an intensity of 0.1 W/cm<sup>2</sup>, and the absorption coefficients for band-to-band transitions and FCA,  $\alpha_{\text{bb}}$  and  $\alpha_{\text{FCA}}$ , both as a function of the photon energy  $E$ . Actually,  $A_{\text{bb}}(E)$  is also a function of the electron and hole concentration, as  $\alpha_{\text{FCA}}(E)$  is proportional to  $n$  and  $p$ . The last term in the denominator of (4) is the external emission rate, which is strictly valid only in the weakly absorbing limit; however, as  $A_{\text{bb}}(E)$  is close to unity in the strong absorbing range, (4) can be used for the whole energy range [4]. Unless stated otherwise,

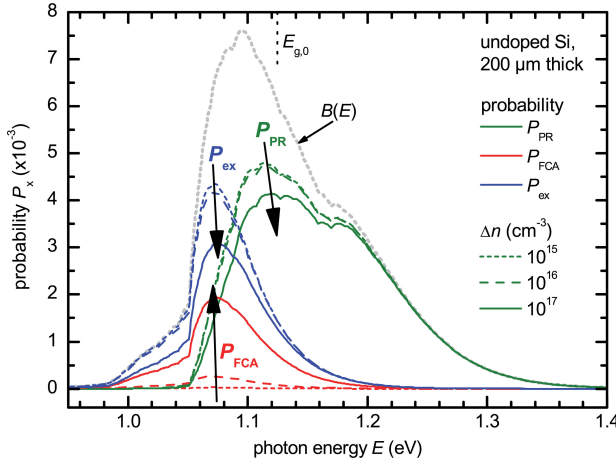


Fig. 2. Spectrally resolved probability for photon-recycling  $P_{PR}$  (band-to-band transitions), free-carrier absorption  $P_{FCA}$ , and external emission  $P_{ex}$  of radiatively emitted photons for different injection levels  $\Delta n$ . The probabilities were calculated for a 200-\$\mu\text{m}\$-thick undoped silicon wafer at 25 °C. Additionally shown is the normalized spectrally resolved spontaneous emission  $B(E)$ . The external emission was calculated by assuming the Lambertian light trapping. The arrows show the increasing contribution of FCA with increasing  $\Delta n$  and its effect on  $P_{PR}$  and  $P_{ex}$ .  $E_{g,0}$  shows the silicon bandgap without BGN.

the solar spectrum of [11] was used, FCA according to [14], and tabulated data for  $n_r$  and  $\alpha_{bb}$  from [13]. Particularly, in Section III-A, the influence of differing parameters will be discussed.

### C. Intrinsic Recombination and Photon Recycling

In Section III-A, we also compare the parameterization of the intrinsic recombination rate of Kerr *et al.*,  $R_{\text{intr},K}$  (see [7, eq. (24)]) with the recently improved description of Richter *et al.*,  $R_{\text{intr},R}$  (see [10, eq. (18)]). Both account for radiative recombination. Each radiative recombination event generates a photon, which has actually a high probability of being reabsorbed by band-to-band transitions in case of the very effective light-trapping assumed here [4], [6]. This reabsorption is also referred to as “photon-recycling” (PR). To account for PR, the radiative recombination coefficient  $B$  in  $R_{\text{intr}}$  is multiplied with  $(1 - P_{PR})$ , where  $P_{PR}$  is the PR probability [6]. Following [4] and [23], we determined  $P_{PR}$  analytically by assuming Lambertian light trapping, as included in (4), also for the luminescent photons to be consistent with the treatment of the incident photons. The resulting  $P_{PR}$  is in good agreement with [24], but differs from the ray-tracing approach of Kerr *et al.* [6], which results, for instance, in a 12% higher  $P_{PR}$  for  $W = 100 \mu\text{m}$  (cf., Fig. 6 in the Appendix). The spectral dependence of the spontaneous emission  $B(E)$ , as required to determine  $P_{PR}$ , was calculated from the generalized Planck equation, which is an extended form of the van Roosbroeck equation [8], [25]. Fig. 2 shows the spectrally resolved probability for photon recycling  $P_{PR}$  (band-to-band transitions), free-carrier absorption  $P_{FCA}$ , and external emission  $P_{ex}$  (calculated from (8) in the Appendix), all for 200-\$\mu\text{m}\$-thick undoped Si at different injection levels. Throughout this study, “undoped” refers to calculations assuming an ultralow doping concentration of  $10^{11} \text{ cm}^{-3}$ . Due to their nature,  $P_{ex}$  dominates the weakly absorbed sub-

bandgap photons, while  $P_{PR}$  dominates at higher photon energies. For injection levels  $\Delta n > 10^{16} \text{ cm}^{-3}$ , FCA becomes significant in the subbandgap range. Although FCA mainly affects  $P_{ex}$ , it also reduces  $P_{PR}$ , particularly under open-circuit conditions due to the high injection levels (cf., Section III-B).

### D. Intrinsic Carrier Concentration

The effective intrinsic carrier concentration  $n_{i,\text{eff}}$  is calculated from the expression [17]

$$n_{i,\text{eff}} = n_{i,0} \exp\left(\frac{\Delta E_g}{2k_B T}\right) \quad (5)$$

with the intrinsic carrier concentration  $n_{i,0}$ , and the BGN  $\Delta E_g$  according to Schenk [16].  $n_{i,\text{eff}}$  is calculated using  $n_{i,0}$  for Si at 300 K of Altermatt *et al.* [17]. As all calculations of this study were performed at 25 °C, the standard testing conditions of silicon solar cells,  $n_{i,0}$ , was scaled using the temperature dependence of Sproul and Green [26], as suggested in [19]. This results in  $n_{i,0} = 8.28 \times 10^9 \text{ cm}^{-3}$  at 25 °C. Fig. 1 shows  $n_{i,\text{eff}}$  as a function of  $\Delta n$  for n-type and p-type Si with different doping concentrations, illustrating the significant increase at high excess carrier densities.

### E. Calculation of I–V Parameters

Finally, the efficiency was calculated numerically by solving (1) iteratively for mpp conditions, i.e., when  $d(JV)/dV$  equals zero. Therefore, (2) is expressed as  $\Delta n(V)$ , to calculate  $R_{\text{intr}}(n_0, p_0, \Delta n(V))$  and  $J_L(n_0, p_0, \Delta n(V))$  in (1). To determine the open-circuit voltage  $V_{OC}$ , (1) was similarly solved for  $J$  equal to zero. The fill factor  $FF$  was calculated from the maximum power,  $V_{OC}$  and the short-circuit current density  $J_{SC}$ .

## III. RESULTS AND DISCUSSION

### A. Influence of the Solar Spectrum and Silicon Parameters

In this section, we address the effect of the following improved modeling parameters on the limiting efficiency: 1) new solar spectrum; 2) updated optical properties of silicon; 3) new parameters for FCA; 4) improved description of the radiative and Auger recombination; and 5) the effect of BGN. We discuss these effects successively. As a starting point, we used a modeling parameter configuration similar to that of Kerr *et al.* [6] with two exceptions: the photon recycling was calculated analytically instead of the ray-tracing approach of Kerr *et al.* (cf., Section II-C and Appendix), and  $n_{i,\text{eff}} = n_{i,0} = 8.28 \times 10^9 \text{ cm}^{-3}$  instead of the  $8.65 \times 10^9 \text{ cm}^{-3}$ , to compare the effect of BGN within one model (cf., Section II-D). The effects are discussed for undoped silicon, as the maximum efficiency is reached in the limit of zero doping [4], [6]. The resulting I–V parameters of this initial modeling configuration are shown in row A of Table I.

In a first step, the old international standard solar spectrum AM1.5G [27] was replaced by the one introduced in [11]. As can be seen from row B of Table I, this increases the maximum efficiency by 0.20%-abs., mainly due to a 0.44 mA/cm<sup>2</sup> increase of  $J_{SC}$ . This  $J_{SC}$  increase is in good

TABLE I  
I–V PARAMETERS AND OPERATION CONDITIONS OF OPTIMUM SILICON SOLAR CELLS UNDER ONE-SUN ILLUMINATION AT 25 °C

Modification	Modeling parameters				$\eta$ (%)	$V_{OC}$ (mV)	$J_{SC}$ (mA/cm <sup>2</sup> )	$FF$ (%)	$V_{mpp}$ (mV)	$\Delta n_{mpp}$ (cm <sup>-3</sup> )	$\Delta n_{OC}$ (cm <sup>-3</sup> )	$W_{opt}$ (μm)		
	$\Phi^a$	$n_r^b$ $\alpha_{bb}^b$	FCA <sup>c</sup>	$R_{intr}^d$										
A	$\Phi_{1st}$	old	$\alpha_{FCA,G}$	$R_{intr,K}$	const.	29.12	769.7	42.75	88.49	700.5	$6.88 \times 10^{15}$	$2.65 \times 10^{16}$	85	
B	spectrum	$\Phi_{2nd}$	old	$\alpha_{FCA,G}$	$R_{intr,K}$	const.	29.32	767.4	43.19	88.47	698.2	$6.58 \times 10^{15}$	$2.53 \times 10^{16}$	95
C	optical properties	$\Phi_{2nd}$	new	$\alpha_{FCA,G}$	$R_{intr,K}$	const.	29.30	767.3	43.16	88.46	698.2	$6.58 \times 10^{15}$	$2.53 \times 10^{16}$	95
D	FCA	$\Phi_{2nd}$	new	$\alpha_{FCA,R}$	$R_{intr,K}$	const.	29.30	767.4	43.16	88.47	698.2	$6.59 \times 10^{15}$	$2.53 \times 10^{16}$	95
E	recombination	$\Phi_{2nd}$	new	$\alpha_{FCA,R}$	$R_{intr,R}$	const.	29.57	767.3	43.31	88.98	700.9	$6.95 \times 10^{15}$	$2.53 \times 10^{16}$	110
F	bandgap narrowing	$\Phi_{2nd}$	new	$\alpha_{FCA,R}$	$R_{intr,R}$	<b>BGN</b>	<b>29.43</b>	761.3	43.31	89.26	697.3	$6.90 \times 10^{15}$	$2.53 \times 10^{16}$	110

The calculation results are compared for different sets of modeling parameters. All resulting operation parameters are specified in the caption of Fig. 4. The respective optimum cell thickness  $W_{opt}$  is also given.

<sup>a</sup> Solar spectrum:  $\Phi_{1st}$  according to [27];  $\Phi_{2nd}$  according to [11].

<sup>b</sup> Refractive index  $n_r$  and absorption coefficient  $\alpha_{bb}$  of silicon: “old” according [28]; “new” according to [13].

<sup>c</sup> Free-carrier absorption (FCA):  $\alpha_{FCA,G}$  according to Green [22];  $\alpha_{FCA,R}$  according to Rüdiger *et al.* [14].

<sup>d</sup> Intrinsic recombination rate of silicon (radiative and Auger recombination):  $R_{intr,K}$  according to Kerr and Cuevas [7];  $R_{intr,R}$  according to Richter *et al.* [10].

<sup>e</sup> Effective intrinsic carrier concentration: “const.” without BGN, i.e.  $n_{i,eff} = n_{i,0} = 8.28 \times 10^9 \text{ cm}^{-3}$ ; “BGN” with BGN according to Schenk [16].

agreement with the 0.5 mA/cm<sup>2</sup> increase observed for experimental silicon solar cell results revised with the new spectrum [12].

Second, the optical properties of silicon [28] were replaced by the more recently published self-consistent dataset of [13]. By comparing row C with the previous row B, no considerable effect on the efficiency (+0.02%-abs.) is observed. This results from the fact that there is no difference in the refractive index  $n_r$  between both, and only a difference of <5% for  $\alpha_{bb}$  in the weakly absorption range, the most relevant range for determining  $J_L$ .

In row D, the FCA parameterization of Green [22] was replaced by the recent parameterization of Rüdiger *et al.* [14]. Again, no considerable effect on the efficiency is observed. Even if there is a certain difference between both, FCA is only a second-order effect, which explains the marginal influence (cf. Section III-B and Fig. 5).

Next, the parameterization of the intrinsic recombination rate  $R_{intr,K}$  [7] is replaced by the recent parameterization  $R_{intr,R}$  [10]. As can be seen from row E,  $R_{intr,R}$  results in a significantly higher efficiency (0.27%-abs.) than  $R_{intr,K}$ , which originates from significantly lower recombination rates for the radiative recombination [8], [9] as well as the Auger recombination [10]. Interestingly, this results not in a higher  $V_{OC}$ , but in a higher  $FF$ , due to the higher mpp voltage  $V_{mpp}$ , and a higher  $J_{SC}$ . The reduced recombination rate leads to an increase of the optimal cell thickness by ~15 μm, which is the reason for the higher  $J_{SC}$ .

Finally, the results of row F were calculated taking BGN for the determination of  $n_{i,eff}$  into account, instead of assuming  $n_{i,eff} = n_{i,0}$  to be constant at  $8.28 \times 10^9 \text{ cm}^{-3}$ . This results in an efficiency reduction of 0.14%-abs., which is mainly due to a 6 mV lower  $V_{OC}$  level and consequently also a lower  $V_{mpp}$  level, while the  $FF$  even increased slightly. The difference in  $V_{mpp}$  of 3.6 mV is in good agreement with the 3.4 mV originally estimated by Tiedje *et al.* [4] for neglecting BGN according to Lanyon and Tuft [29].

Altogether, row F represents the I–V parameters for the optimum silicon solar cell calculated with state-of-the-art mod-

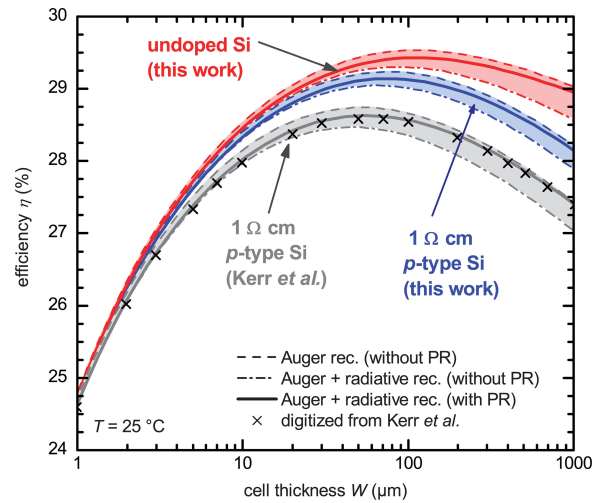


Fig. 3. Efficiency as a function of the thickness for silicon solar cells under 1-sun illumination and at 25 °C. The solid lines represent the efficiency for a cell made of 1 Ω·cm p-type Si and undoped Si, taking the radiative and Auger recombination, as well as photon recycling (PR) into account. The additional curves show cells constrained either only by the Auger recombination or by the Auger and radiative recombination. Both are calculated without taking PR into account and, thus, represent an upper limit assuming complete photon recycling and lower limit assuming no photon recycling, respectively. All these curves were calculated with the modeling parameters listed in row F of Table I. Additionally, the curves are also shown for 1 Ω·cm p-type Si calculated with the modeling parameters used by Kerr and Cuevas [6]. The cross symbols are the respective data points digitized from [6, Fig. 2].

eling parameters. The resulting efficiency limit is 29.43%, 0.38%-abs. higher than the 29.05% calculated by Kerr *et al.* [6]. Fig. 3 shows the limiting efficiency calculated with these modeling parameters as a function of the cell thickness for undoped Si, as discussed so far, as well as for 1 Ω·cm p-type Si. The 1 Ω·cm p-type Si calculation by Kerr *et al.* (see [6, Fig. 2]) is also included. The latter results in a peak efficiency of 28.6%, which is 0.54%-abs. lower than the 29.14% of this work. Thus, the difference is even more pronounced for higher doping concentration.

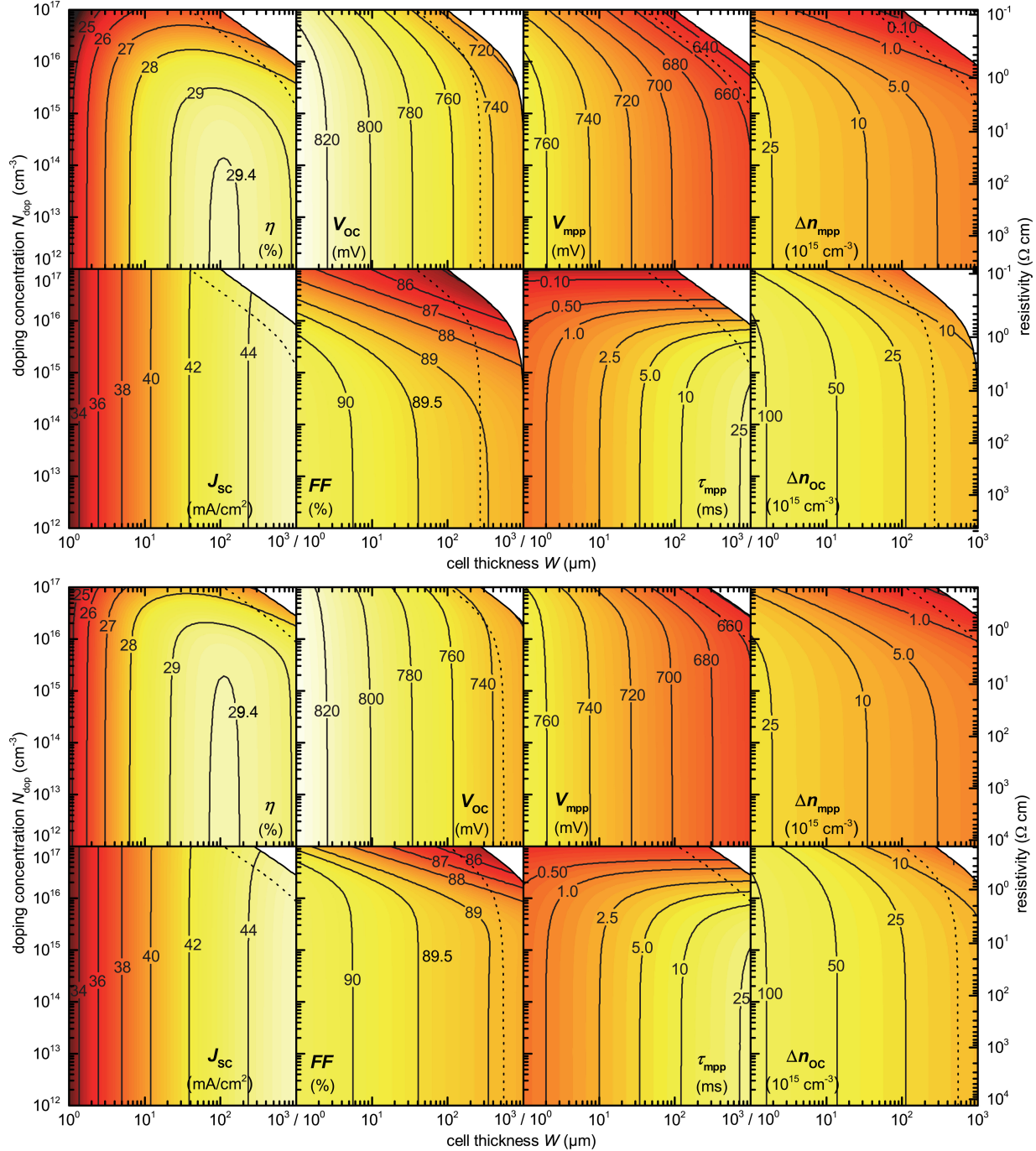


Fig. 4. Limiting efficiency and  $I$ - $V$  parameters of n-type Si (upper graphs) and p-type Si (lower graphs) solar cells as a function of the cell thickness and the doping concentration. The results are calculated for cells under 1-sun illumination (AM1.5G) at 25 °C, which are constrained by the radiative and Auger recombination taking photon recycling and FCA into account. The modeling parameters of row F in Table I were used for these calculations. In addition to the efficiency  $\eta$ , also shown are the open-circuit voltage  $V_{\text{OC}}$ , the voltage at the maximum power point  $V_{\text{mpp}}$ , the short-circuit current density  $J_{\text{SC}}$ , the fill factor  $FF$ , the effective lifetime at mpp  $\tau_{\text{mpp}}$ , as well as the injection levels at mpp and OC,  $\Delta n_{\text{mpp}}$  and  $\Delta n_{\text{OC}}$ , respectively. The ratio of the minority carrier diffusion length  $L$  and the thickness,  $L/W$ , is  $<2$  in the white upper-right corner of each plot, and  $<5$  right to the dashed line. As discussed in the text, these ranges have limited accuracy due to the narrow-base approximation.

Fig. 3 also shows upper and lower bounds for the efficiency, which were calculated assuming complete and no photon recycling, respectively. For the weakly absorbed luminescence light of the radiative recombination, the silicon absorbance and consequently the photon recycling increases considerable with increasing cell thickness (cf., Fig. 6 in the Appendix). For that

reason, the resulting efficiency curve with photon recycling is close to the lower bound for thin cells, and converges to the upper bound for thick cells. For 1  $\Omega\cdot\text{cm}$  p-type Si, the calculation of Kerr *et al.* results in a higher difference between both bounds (35% higher at 80  $\mu\text{m}$ ), which directly reflects the higher radiative recombination rate included in  $R_{\text{intr},K}$ .

### B. Influence of Base Doping Concentration

The results discussed in the previous section reveal a significant influence of  $R_{\text{intr}}$  and  $n_{i,\text{eff}}$  on the limiting efficiency, both strongly affected by the base doping concentration  $N_{\text{dop}}$ . Thus, the limiting efficiency will also vary considerably with  $N_{\text{dop}}$ . Fig. 4 shows the limiting efficiency as well as the  $I$ - $V$  parameters for n-type and p-type Si cells as a function of  $N_{\text{dop}}$  and  $W$ , using the state-of-the-art modeling parameters as listed in row F of Table I, particularly taking also BGN into account. It is important to note that the narrow-base approximation used throughout this study to relate the cell voltage with  $\Delta n$  according to (2) is strictly valid only for  $W \ll L$ , with  $L$  being the minority carrier diffusion length [3]. If  $L$  is in the same order as  $W$  or even smaller, nonuniform charge carrier profiles lead to significant gradients in the minority carrier quasi-Fermi levels, which affects the cell voltage. The device simulator PC1D [30] was used to estimate roughly the influence of minority carrier quasi-Fermi level gradients on the cell voltage. According to this simulation, the effect on the voltage is  $<2.5$  mV for  $L/W > 2$ , and  $<0.3$  mV for  $L/W > 5$ .<sup>1</sup> These ranges are also shown in Fig. 4:  $L/W < 2$  in the white upper-right corner of each plot, and  $<5$  right to the dashed line. Note that the results at the mpp are less influenced than at open-circuit conditions, due to the higher effective lifetime at mpp,  $\tau_{\text{mpp}}$ , which is associated with the lower injection level at mpp,  $\Delta n_{\text{mpp}}$ . In particular, for the absolute limiting efficiency calculation discussed in Section III-A, the narrow-base assumption is well valid [3], [4].

As expected, the limiting efficiency  $\eta$  for n-type and p-type Si cells shown in Fig. 4 reaches the maximum in the limit of undoped Si with a thickness of  $\sim 110$   $\mu\text{m}$ . For lower thicknesses,  $\eta$  increases with increasing  $W$  due to improved light absorption quantified by  $J_{\text{SC}}$ . Although  $\Delta n_{\text{mpp}}$  decreases with increasing  $W$ , which results in an increasing  $\tau_{\text{mpp}}$ ,  $V_{\text{mpp}}$  and also  $V_{\text{OC}}$  decrease with increasing  $W$  due to an increasing total recombination current density  $qWR_{\text{intr}}$  in (1). This increasing total recombination compensates the benefit of increasing  $J_{\text{SC}}$  at high thicknesses, and consequently decreases  $\eta$  again.  $R_{\text{intr}}$  also increases with increasing  $N_{\text{dop}}$ , particularly above  $\sim 10^{15}$   $\text{cm}^{-3}$  in the case of n-type Si and above  $\sim 10^{16}$   $\text{cm}^{-3}$  in the case of p-type Si. This leads to a reduction of  $V_{\text{mpp}}$  and  $V_{\text{OC}}$  with increasing  $N_{\text{dop}}$ , which is more pronounced for n-type Si mainly due to the different recombination kinetics of the low injection Auger recombination processes.

To illustrate the influence of the doping concentration, Fig. 5 shows the loss current density at the maximum power point,  $J_{\text{loss,mpp}}$ , as a function of  $N_{\text{dop}}$  for n-type Si cells with a thickness of 110  $\mu\text{m}$ .  $J_{\text{loss,mpp}}$  is separated into the contributions of the incident photons absorbed by free carriers  $J_{\text{FCA}}$ , the recombination current of Auger recombination, separated into the low- and high-injection contribution,  $J_{\text{A,li}}$  and  $J_{\text{A,hi}}$ , respectively, as well as the effective radiative recombination  $J_{\text{rad,eff}}$ , which is reduced by the fraction of recycled photons. The current density of the recycled photons  $J_{\text{rad,PR}}$  is shown too as a dashed area above  $J_{\text{loss,mpp}}$ .

<sup>1</sup>  $L$  was calculated using the mobility model of Klaassen [31].

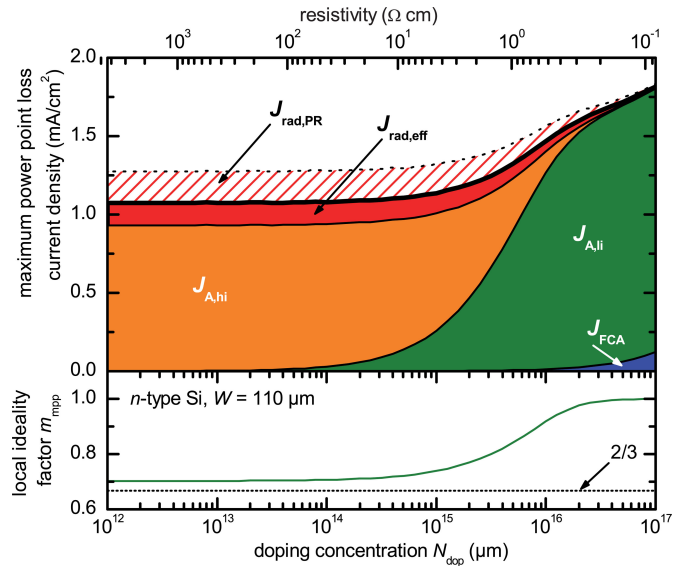


Fig. 5. Loss current density at the maximum power point  $J_{\text{loss,mpp}}$  (thick black line, upper graph) as a function of the doping concentration  $N_{\text{dop}}$  for ideal n-type Si solar cells with a thickness of 110  $\mu\text{m}$ . The contribution of the incident photons absorbed by free-carriers  $J_{\text{FCA}}$ , the recombination current of the Auger recombination, separated into the low- and high-injection contribution,  $J_{\text{A,li}}$  and  $J_{\text{A,hi}}$ , respectively, as well as the effective radiative recombination  $J_{\text{rad,eff}}$ , which is reduced by the fraction of recycled photons, are shown. The current density of this recycled photons  $J_{\text{rad,PR}}$  is shown too as a dashed area above  $J_{\text{loss,mpp}}$ . The lower graph shows the local ideality factor  $m_{\text{mpp}}$  evaluated at mpp.

The Auger recombination clearly dominates the whole  $N_{\text{dop}}$  range particularly as a distinct part of the radiative recombining charge carriers are recycled. While at low doping concentrations  $J_{\text{A,hi}}$  dominates,  $J_{\text{A,li}}$  dominates at high doping concentrations, which directly reflects the transition from high injection to low injection at mpp (cf.,  $\Delta n_{\text{mpp}}$  in Fig. 4). Although there is a small contribution of FCA for  $N_{\text{dop}} > 10^{16}$   $\text{cm}^{-3}$ , the main increase of  $J_{\text{loss,mpp}}$  with increasing  $N_{\text{dop}}$  is caused by the absolute increasing contribution of the Auger recombination.

From Fig. 4, it can be seen that the fill factor (FF) decreases with increasing  $N_{\text{dop}}$ , in the case of the n-type cells significantly above  $10^{15}$   $\text{cm}^{-3}$ . If series resistances are negligible, as assumed, the FF is mainly influenced by the  $V_{\text{OC}}$  and the cell ideality factor  $m$  [32]. To some extent, therefore, the FF reduction can be explained by the  $V_{\text{OC}}$  reduction at high doping concentrations. However, it is well known that  $m$  can vary significantly with the doping and injection level. According to the free-particle Auger model, the ideality factor of cells limited by the Auger recombination is reduced from unity under low injection conditions to 2/3 under high injection conditions, which results in a significant increase of the upper FF bound [3]. To analyze the ideality factor for the cell simulations of this study, we fitted the one-diode equation

$$J = J_L - J_0 \left[ \exp \left( \frac{V}{mV_T} \right) - 1 \right] \quad \text{with} \quad V_T = \frac{k_B T}{q} \quad (6)$$

to the modeled  $I$ - $V$  characteristics in a voltage range around  $V_{\text{mpp}}$  by varying  $m$  and the recombination prefactor  $J_0$ . This yields the local ideality factor at the maximum power point

$m_{\text{mpp}}$ . The resulting dependence of  $m_{\text{mpp}}$  on  $N_{\text{dop}}$  is shown exemplary for the 110-nm-thick n-type Si cells in the lower graph of Fig. 5. As expected,  $m_{\text{mpp}}$  directly correlates with the transition from high to low injection quantified by the transition from  $J_{A,\text{hi}}$  to  $J_{A,\text{li}}$ . Similar to the free-particle Auger model,  $m_{\text{mpp}}$  converges to unity in the case of low injection, and is with 0.70 close to 2/3 under high injection. Actually, a value slightly higher than 2/3 is expected, as the denominator of the factor 2/3 originates from the exponent of the charge carrier dependence of the high injection Auger recombination, which is 2.92 in  $R_{\text{intr,R}}$  [10]. This shows that for cells in high injection, the bound on the fill factor is increased similarly to the known increase of the free-particle Auger model.

#### IV. CONCLUSION

This study has presented new calculations of the limiting efficiency for crystalline silicon solar cells (in the “narrow base” approximation) systematically as a function of the doping concentration and the cell thickness taking recently improved modeling parameters into account. A detailed analysis revealed significant effects of the new international standard solar spectrum and the improved quantitative description of the Coulomb-enhanced radiative and Auger recombination, while improved optical properties of silicon and a new parameterization for free-carrier absorption (FCA) have only a minor influence. The limiting efficiency was also observed to be affected by BGN particularly due to the high-injection conditions at mpp. Applying the state-of-the-art modeling parameters results in a maximum theoretical efficiency of 29.43% for a 110- $\mu\text{m}$ -thick cell made of undoped Si. An evaluation of the loss current density at mpp reconfirms a dominating effect of the Auger recombination, while the FCA contribution vanishes for doping concentrations below  $10^{16} \text{ cm}^{-3}$ , and the contribution of the radiative recombination is rather small due to photon recycling.

#### APPENDIX DETERMINATION OF THE PHOTON RECYCLING

To determine the photon recycling probability  $P_{\text{PR}}$ , the spectrally resolved radiative recombination coefficient  $B(E)$  was calculated from the generalized Planck equation [8], [25]

$$B(E) = \frac{1}{\pi^2 c_0^2 \hbar^3 n_{\text{i,eff}}^2} n_{\text{r}}^2(E) E^2 \alpha_{\text{bb}}(E) \exp\left(-\frac{E}{k_{\text{B}} T}\right) \quad (7)$$

with the photon energy  $E$ .  $P_{\text{PR}}$  is then determined by evaluating numerically

$$P_{\text{PR}}(W, n, p) = \frac{\int_0^\infty A_{\text{bb}}(E, W, n, p) B(E) dE}{\int_0^\infty B(E) dE}. \quad (8)$$

FCA is a function of  $n$  and  $p$ , and consequently also  $A_{\text{bb}}$  given in (4) and  $P_{\text{PR}}$ . The probability for FCA or external emission is calculated by replacing  $A_{\text{bb}}$  with the respective term analogous to the calculation of  $A_{\text{bb}}$  in (4). It is worth mentioning that the denominator of (8) results in  $B = 4.82 \times 10^{15} \text{ cm}^3 \cdot \text{s}^{-1}$  when using  $\alpha_{\text{bb}}(E)$  of Green *et al.* [13] in (7). This value is in good agreement with the  $4.73 \times 10^{15} \text{ cm}^3 \cdot \text{s}^{-1}$  determined by Trupke

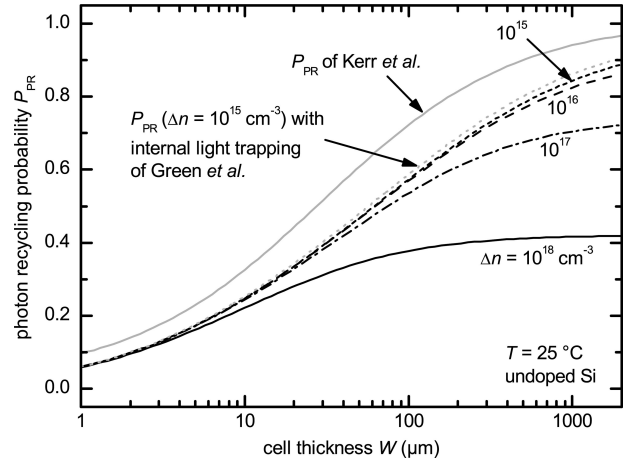


Fig. 6. Photon recycling probability  $P_{\text{PR}}$  for undoped Si as a function of the wafer thickness for different injection levels  $\Delta n$ .  $P_{\text{PR}}$  was calculated assuming the Lambertian light trapping according to Tiedje *et al.* [4] and taking parasitic free-carrier absorption into account. For  $\Delta n = 10^{15} \text{ cm}^{-3}$ ,  $P_{\text{PR}}$  was also exemplary calculated with Lambertian light trapping according to Green *et al.* [24].  $P_{\text{PR}}$  published by Kerr *et al.* determined with ray tracing simulations [6] is also shown.

*et al.* [8], which is also included in  $R_{\text{intr,R}}$  of Richter *et al.* [10], indicating consistency.

Fig. 6 shows  $P_{\text{PR}}$  as a function of the cell thickness  $W$  for different injection levels  $\Delta n$  of undoped Si. The decreasing  $P_{\text{PR}}$  with increasing  $\Delta n$  is caused by the increasing parasitic FCA, as can be seen from Fig. 2. Below  $\Delta n = 10^{15} \text{ cm}^{-3}$ ,  $P_{\text{PR}}$  remains at the same level as for  $\Delta n = 10^{15} \text{ cm}^{-3}$ , because FCA is negligible for such low charge carrier concentrations (cf., Fig. 2). Fig. 6 shows additionally  $P_{\text{PR}}$  according to Green *et al.* [24] (Lambertian light trapping) exemplarily for  $\Delta n = 10^{15} \text{ cm}^{-3}$ , as well as  $P_{\text{PR}}$  of the ray-tracing approach of Kerr *et al.* (digitized from Fig. 1 of [6]). While the  $P_{\text{PR}}$  applied in this work is in good agreement with Green *et al.*, it is more conservative than the  $P_{\text{PR}}$  of Kerr *et al.*, particularly around 100  $\mu\text{m}$ , the thickness of the optimum Si solar cell.

#### ACKNOWLEDGMENT

The authors would like to thank Dr. P. Campbell for valuable discussions about photon recycling.

#### REFERENCES

- [1] K. Maki, D. Fujishima, H. Inoue, Y. Tsunomura, T. Asaumi, S. Taira, T. Kinoshita, M. Taguchi, H. Sakata, H. Kanno, and E. Maruyama, “High-efficiency HIT solar cells with a very thin structure enabling a high  $V_{\text{OC}}$ ,” presented at the 37th IEEE Photovoltaic Specialists Conf., Seattle, WA, USA, 2011.
- [2] W. Shockley and H. J. Queisser, “Detailed balance limit of efficiency of p-n junction solar cells,” *J. Appl. Phys.*, vol. 32, pp. 510–9, 1961.
- [3] M. A. Green, “Limits on the open-circuit voltage and efficiency of silicon solar cells imposed by intrinsic Auger processes,” *IEEE Trans. Electron Devices*, vol. ED-31, no. 5, pp. 671–678, May 1984.
- [4] T. Tiedje, E. Yablonovitch, G. D. Cody, and B. G. Brooks, “Limiting efficiency of silicon solar cells,” *IEEE Trans. Electron Devices*, vol. ED-31, no. 5, pp. 711–716, May 1984.
- [5] A. Hangleiter and R. Häcker, “Enhancement of band-to-band Auger recombination by electron-hole correlations,” *Phys. Rev. Lett.*, vol. 65, pp. 215–18, 1990.

- [6] M. J. Kerr, A. Cuevas, and P. Campbell, "Limiting efficiency of crystalline silicon solar cells due to Coulomb-enhanced Auger recombination," *Prog. Photovolt: Res. Appl.*, vol. 11, pp. 97–104, 2003.
- [7] M. J. Kerr and A. Cuevas, "General parameterization of Auger recombination in crystalline silicon," *J. Appl. Phys.*, vol. 91, p. 2473, 2002.
- [8] T. Trupke, M. A. Green, P. Würfel, P. P. Altermatt, A. Wang, J. Zhao, and R. Corkish, "Temperature dependence of the radiative recombination coefficient of intrinsic crystalline silicon," *J. Appl. Phys.*, vol. 94, p. 4930, 2003.
- [9] P. P. Altermatt, F. Geelhaar, T. Trupke, X. Dai, A. Neisser, and E. Daub, "Injection dependence of spontaneous radiative recombination in crystalline silicon: Experimental verification and theoretical analysis," *Appl. Phys. Lett.*, vol. 88, pp. 261901-1–261901-3, 2006.
- [10] A. Richter, S. W. Glunz, F. Werner, J. Schmidt, and A. Cuevas, "Improved quantitative description of Auger recombination in crystalline silicon," *Phys. Rev. B*, vol. 86, p. 165202, 2012.
- [11] *Photovoltaic Devices—Part 3: Measurement Principles for Terrestrial Photovoltaic (Pv) Solar Devices With Reference Spectral Irradiance Data*, Int. Stand., IEC 60904-3, 2nd ed., 2008.
- [12] M. A. Green, K. Emery, Y. Hishikawa, and W. Warta, "Solar cell efficiency tables (version 33)," *Prog. Photovolt: Res. Appl.*, vol. 17, pp. 85–94, 2009.
- [13] M. A. Green, "Self-consistent optical parameters of intrinsic silicon at 300 K including temperature coefficients," *Sol. Energy Mater. Sol. Cells*, vol. 92, pp. 1305–10, 2008.
- [14] M. Rüdiger, J. Greulich, A. Richter, and M. Hermle, "Parameterization of free carrier absorption in highly doped silicon for solar cells," *IEEE Trans. Electron Devices*, vol. 60, no. 7, p. 2156, Jul. 2013.
- [15] J. Mattheis, J. H. Werner, and U. Rau, "Finite mobility effects on the radiative efficiency limit of pn-junction solar cells," *Phys. Rev. B*, vol. 77, p. 085203, 2008.
- [16] A. Schenk, "Finite-temperature full random-phase approximation model of band gap narrowing for silicon device simulation," *J. Appl. Phys.*, vol. 84, pp. 3684–3695, 1998.
- [17] P. P. Altermatt, A. Schenk, F. Geelhaar, and G. Heiser, "Reassessment of the intrinsic carrier density in crystalline silicon in view of band-gap narrowing," *J. Appl. Phys.*, vol. 93, p. 1598, 2003.
- [18] P. P. Altermatt, "Models for numerical device simulations of crystalline silicon solar cells—A review," *J. Comput. Electron.*, vol. 10, pp. 314–330, 2011.
- [19] A. Wolf, D. Biro, J.-F. Nekarda, S. Stumpp, A. Kimmerle, S. Mack, and R. Preu, "Comprehensive analytical model for locally contacted rear surface passivated solar cells," *J. Appl. Phys.*, vol. 108, pp. 1–13, 2010.
- [20] M. A. Green, "Limiting efficiency of bulk and thin-film silicon solar cells in the presence of surface recombination," *Prog. Photovolt: Res. Appl.*, vol. 7, pp. 327–30, 1999.
- [21] S. Kolodinski, J. H. Werner, T. Wittchen, and H. J. Queisser, "Quantum efficiencies exceeding unity due to impact ionization in silicon solar cells," *Appl. Phys. Lett.*, vol. 63, p. 2405, 1993.
- [22] M. A. Green, *Silicon Solar Cells: Advanced Principles and Practice*. Sydney, N.S.W., Australia: Centre for Photovoltaic Devices and Systems UNSW, 1995.
- [23] O. D. Miller, E. Yablonovitch, and S. R. Kurtz, "Strong internal and external luminescence as solar cells approach the Shockley–Queisser limit," *IEEE J. Photovoltaics*, vol. 2, no. 3, pp. 303–311, Jul. 2012.
- [24] M. A. Green, J. Zhao, A. Wang, P. J. Reece, and M. Gal, "Efficient silicon light-emitting diodes," *Nature*, p. 805, 2001.
- [25] P. Würfel, "The chemical potential of radiation," *J. Phys. C: Solid State Phys.*, vol. 15, pp. 3967–3985, 1982.
- [26] A. B. Sproul and M. A. Green, "Intrinsic carrier concentration and minority-carrier mobility of silicon from 77 to 300 K," *J. Appl. Phys.*, vol. 73, p. 1213, 1993.
- [27] *Photovoltaic Devices—Part 3: Measurement Principles For Terrestrial Photovoltaic (Pv) Solar Devices With Reference Spectral Irradiance Data*, Int. Stand., IEC 60904-3, 1st ed., 1989.
- [28] M. A. Green and M. J. Keevers, "Optical properties of intrinsic silicon at 300 K," *Prog. Photovolt: Res. Appl.*, vol. 3, pp. 189–192, 1995.
- [29] H. P. D. Lanyon and R. A. Tuft, "Bandgap narrowing in moderately to heavily doped silicon," *IEEE Trans. Electron. Devices*, vol. ED- 26, no. 7, pp. 1014–1018, Jul. 1979.
- [30] D. A. Clugston and P. A. Basore, "PC1D version 5: 32-bit solar cell modeling on personal computers," presented at the 26th IEEE Photovoltaic Specialists Conf., Anaheim, CA, USA, 1997.
- [31] D. B. M. Klaassen, "A unified mobility model for device simulation—Part I: Model equations and concentration dependence," *Solid-State Electron.*, vol. 35, pp. 953–959, 1992.
- [32] M. A. Green, "Accuracy of analytical expressions for solar cell fill factors," *Solar Cells*, vol. 7, pp. 337–340, 1982.



**Armin Richter** received the Diploma degree in physics from the University of Hamburg, Hamburg, Germany, in 2008. He is currently working toward the Ph.D. degree from the Fraunhofer Institute for Solar Energy Systems, Freiburg, Germany.



**Martin Hermle** received the Diploma degree in physics from the University of Karlsruhe, Karlsruhe, Germany, in 2003 and the Ph.D. degree in physics from the University of Konstanz, Konstanz, Germany, in 2008.

He joined the Fraunhofer-Institute for Solar Energy Systems, Freiburg, Germany, in 2002. Since 2008, he has been the Head of the Department of High Efficiency Silicon Solar Cell. His research interests include the development of solar cell technologies for high-efficiency silicon solar cells and the analysis, characterization, and modelling of silicon and III/V solar cells.



**Stefan W. Glunz** (M'10) received the Ph.D. degree from the University of Freiburg, Freiburg, Germany, in 1995.

He is the Director of the "Solar Cells—Development and Characterization" Division, Fraunhofer Institute for Solar Energy Systems, Freiburg, Germany. His research interests include the design, fabrication, and analysis of high-efficiency silicon solar cells. Among other scientific and technological achievements, his group has set the actual world record for solar cells on multicrystalline silicon. He is the author/co-author of more than 90 journal and 250 conference papers.

Dr. Glunz is the Founding Editor of IEEE JOURNAL OF PHOTOVOLTAICS. In 2008, he received the Eni Award for the promotion of science and technology in the field of renewable energies. He is a scientific committee member for several conferences and workshops in the field of solar energy.